


Article

Development of Functional Thyroid C Cell-like Cells from Human Pluripotent Cells in 2D and in 3D Scaffolds

Kwaku Dad Abu-Bonsrah ^{1,2,*} , Donald F. Newgreen ^{1,*,†} and Mirella Dottori ^{3,4,*,†}¹ The Murdoch Children's Research Institute, Royal Children's Hospital, Parkville, VIC 3052, Australia² Department of Paediatrics, University of Melbourne, Parkville, VIC 3010, Australia³ Department of Biomedical Engineering, Department of Anatomy and Neurosciences, University of Melbourne, Parkville, VIC 3010, Australia⁴ Illawarra Health and Medical Research Institute, School of Medicine, Molecular Horizons, University of Wollongong, Wollongong, NSW 2522, Australia

* Correspondence: k.abu@florey.edu.au (K.D.A.-B.); donnew@westnet.com.au (D.F.N.); mdottori@uow.edu.au (M.D.)

† Co-senior authors.

Abstract: Medullary thyroid carcinoma contributes to about 3–4% of thyroid cancers and affects C cells rather than follicular cells. Thyroid C cell differentiation from human pluripotent stem cells has not been reported. We report the stepwise differentiation of human embryonic stem cells into thyroid C cell-like cells through definitive endoderm and anterior foregut endoderm and ultimobranchial body-like intermediates in monolayer and 3D Matrigel culture conditions. The protocol involved sequential treatment with interferon/transferrin/selenium/pyruvate, foetal bovine serum, and activin A, then IGF-1 (Insulin-like growth factor 1), on the basis of embryonic thyroid developmental sequence. As well as expressing C cell lineage relative to follicular-lineage markers by qPCR (quantitative polymerase chain reaction) and immunolabelling, these cells by ELISA (enzyme-linked immunoassay) exhibited functional properties in vitro of calcitonin storage and release of calcitonin on calcium challenge. This method will contribute to developmental studies of the human thyroid gland and facilitate in vitro modelling of medullary thyroid carcinoma and provide a valuable platform for drug screening.

Keywords: pluripotent stem cells; endoderm; disease modelling; thyroid C cells



Citation: Abu-Bonsrah, K.D.; Newgreen, D.F.; Dottori, M. Development of Functional Thyroid C Cell-like Cells from Human Pluripotent Cells in 2D and in 3D Scaffolds. *Cells* **2021**, *10*, 2897. <https://doi.org/10.3390/cells10112897>

Academic Editor:
Kai-Christian Sonntag

Received: 10 September 2021
Accepted: 21 October 2021
Published: 26 October 2021

Publisher's Note: MDPI stays neutral with regard to jurisdictional claims in published maps and institutional affiliations.



Copyright: © 2021 by the authors. Licensee MDPI, Basel, Switzerland. This article is an open access article distributed under the terms and conditions of the Creative Commons Attribution (CC BY) license (<https://creativecommons.org/licenses/by/4.0/>).

1. Introduction

Thyroid cancer is a malignant tumour of the endocrine system and the most common of the endocrine cancers, accounting for 1% of newly diagnosed cancers [1]. Malignant thyroid cancers can be categorised as differentiated of follicular cell origin (papillary, follicular, and Hürthle cell), less differentiated of C cell origin (medullary thyroid carcinoma or MTC) and mostly hereditary [2], and undifferentiated and aggressive (anaplastic) [3].

Statistics in both the USA and Australia show that the incidence of thyroid cancer detection is increasing faster than that of other solid tumours with a 3:1 preponderance of females (Australian Government Cancer Statistics) [4]. In the USA, about 40,000 female and 13,000 male new cases were estimated regarding individuals diagnosed with thyroid cancer in 2018, with about 1.2% of adults having this diagnosis at some time in their lifetime [5,6]. Reports show the rise in incidence of differentiated thyroid cancers in children and teens as well as adults [7,8]. Thyroid cancers may show comorbidities; for example, pheochromocytoma and parathyroid adenoma frequently occur with MTC in multiple endocrine neoplasia type 2 [9], and the incidence of MTC is elevated in patients with the neural defect of the distal colon, Hirschsprung disease [10].

MTC results mainly from somatic or germline mutation in the RET (rearranged during transfection) proto-oncogene [11] and contributes to about 3–4% of thyroid cancers [12]. It is

a distinct thyroid cancer which originates from thyroid C cells and has a strongly metastatic potential. C cells are located outside the thyroid follicles and are hence referred to as parafollicular. The C cells produce calcitonin, a hormone that regulates Ca^{2+} metabolism by lowering blood Ca^{2+} levels [13,14], in opposition to the effects of parathyroid hormone (Poole and Reeve, 2005).

Treatment of MTC is typically thyroidectomy and often also with local lymph node removal. This radical surgery dates back over 100 years and is intricate with real danger of collateral damage [15,16]. Radiotherapy is frequently recommended as follow-up treatment. Tyrosine kinase inhibitors vandetanib and cabozantinib, which inhibit the RET growth factor receptor, have been approved by the U.S. Food and Drug Administration; however, RET was not the intended target, and these drugs also have powerful inhibitory effects on other receptors such as VEGFR (vascular endothelial growth factor receptor), EGFR (epidermal growth factor receptor), MET (mesenchymal to epithelial transition), KIT (KIT proto-oncogene, receptor tyrosine kinase), FLT3 (FMS-like tyrosine kinase 3), TIE-2 (tyrosine kinase with immunoglobulin-like loops and epidermal growth factor homology domain-2), TRKB (tropomyosin receptor kinase B), and AXL (AXL receptor tyrosine kinase) [17,18]. Because of these side effects, they are used with caution and only for the most aggressive forms of MTC, and therefore improvements in pharmacological therapeutics would be welcomed.

Disease modelling in the human cell context provides the platform to better understand and find appropriate therapeutic measures [19–22]. Generating a disease model specifically for MTCs requires a differentiation protocol for the affected cell type, thyroid C cells.

There has been much research on the differentiation of derivatives of the foregut endoderm, including lung progenitors [23] and thymus progenitors [24]. Work on the thyroid focusses on follicular cells, and methods are available for production and differentiation of these cells in vitro from pluripotent cells [25,26]. There is less information about the differentiation of C cells, and even their embryonic origin has had to be drastically revised. Unlike follicular cells, thyroid C cells do not arise from the thyroid *anlage* but rather from the ultimobranchial body (ubb) during embryonic development [27] and differentiate into functional C cells in mammals once the ubb fuses with the thyroid [28–30] (Figure 1). In non-mammalian vertebrates, this fusion does not occur [31]. Previously, C cell progenitors were viewed as being of neural crest origin [32], and this fitted with the permanent or transient expression of a suite of markers associated with neurons such as serotonin (5HT) receptor, somatostatin receptor, calcitonin gene-related peptide (CGRP), β -III tubulin (TUJ1), PGP9.5, and many others, as well as neurotransmitter storage vesicles [29,33]. However, recent research on the embryonic origin, development, and differentiation of mouse and human thyroid C cells in vivo proved that in mammals C cells originate from foregut endoderm [29,34] and can be classed as enteroendocrine cells.

The use of 3D cell culture methods has opened many avenues to better understand how cells reorganise to form tissues, how different cell types interact, and how cells respond to external stimuli such as drugs and hormones. These techniques have been used in stem cell biology to study organogenesis and in cancer biology to study angiogenesis, metastasis, and drug screening since 3D models mimic the in vivo environment in terms of attaining appropriate tissue architecture with improved cell differentiation and functionality [35–37].

Here, we show a novel differentiation method for deriving functional human thyroid C cell-like cells in vitro via foregut endoderm-like intermediate steps followed by neural-like induction conditions using 2D and 3D scaffold techniques. These cells should prove useful models for detailed studies of human C cell differentiation as well as providing human cellular models for diseases such as MTC which affect this cell type.

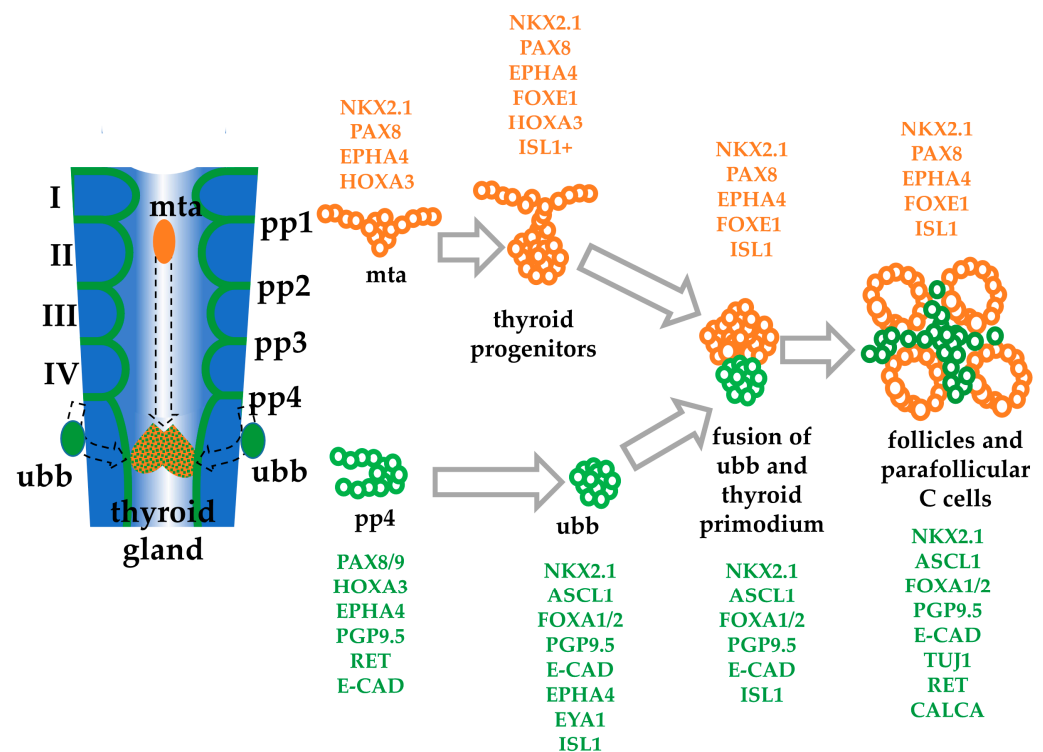


Figure 1. Development of the thyroid organ. Scheme of the development of the pharynx showing the origin and morphogenetic movements of the medial thyroid *anlage* (mta) from the midventral pharynx, and the ultimobranchial body (ubb) from pharyngeal pouch 4 (pp4). These migrate and fuse to form the follicular and parafollicular C cells, respectively, of the mammalian thyroid gland. These moieties remain separate in other vertebrates. Roman numbers indicate the pharyngeal arches. Key genes are indicated in orange (thyroid follicular cell differentiation) and green (thyroid parafollicular C cell differentiation) [25,38].

2. Materials and Methods

2.1. Ethics Statement

All experiments were performed with the approval from the Murdoch Children's Research Institute Institutional Biosafety Committee 226-2015 PC2. Human Stem Cell studies were performed with approval from University of Melbourne Human Ethics, ID 1545384, 0605017 and 1545394.

2.2. Human Embryonic Stem Cells, hESC Culture, and Thyroid C Cell Differentiation in 2D Cultures

hESCs (H9, WiCell; HES3, ESI International; 007 iPSC, kindly provided by Alice Pébay, Centre for Eye Research Australia) were cultured to 80–90% confluence and harvested using EDTA-PBS buffer for 4–6 min. The buffer was gently removed, and 2 mL of medium was gently added to harvest the cells into a 15 mL Falcon tube, and 10 μ L was counted using a haemocytometer (Thermo Fisher Scientific, North Ryde, Australia). Cells were seeded as a monolayer at 1×10^5 on Matrigel-coated organoid culture dishes with TESR™-E8™ complete media supplemented with 3.2 μ g/mL (10 μ M) Y-27632 (Sigma-Aldrich, Castle Hill, Australia) and cultured at 37 °C and 5% CO₂ in a humidified incubator overnight; this was recorded as day 0 (see Figure 2a). On day 1, the media was changed to DMEM/F12 supplemented with 0.5% foetal bovine serum (FBS) and 100 ng/mL (3.82 nM dimer) HumanKine Activin A (Miltenyi Biotec, Macquarie Park, Australia) with 1X ITS-A (insulin–transferrin–selenium–sodium pyruvate, Thermo Fisher Scientific) and cultured at 37 °C and 5% CO₂ in a humidified incubator for 5 days. Medium was replaced on days 3, 4 and 5. On day 6, the media was changed to DMEM/F12 supplemented with 10% FBS, 1% pen–strep, 1X ITS-A with 2 ng/mL (261.5 pM) recombinant human IGF-1 protein, carrier-free (R&D

systems - In Vitro Technologies, Lane Cove West, Australia) or 3 ng/mL (10 nM) retinoic acid, RA (Sigma-Aldrich) for 6 days (until day 12) or with both IGF-1 and RA. Medium change was done every other day until day 12, where the cells were cultured without IGF-1 or RA for 3 days, until day 15. The cells spontaneously formed domes/nodules around days 10–11. On day 15, cells were assayed for calcitonin by ELISA (see below) before cells were harvested for RNA extraction. Parallel cultures for immunofluorescence staining were fixed and stained following the protocols outlined below.

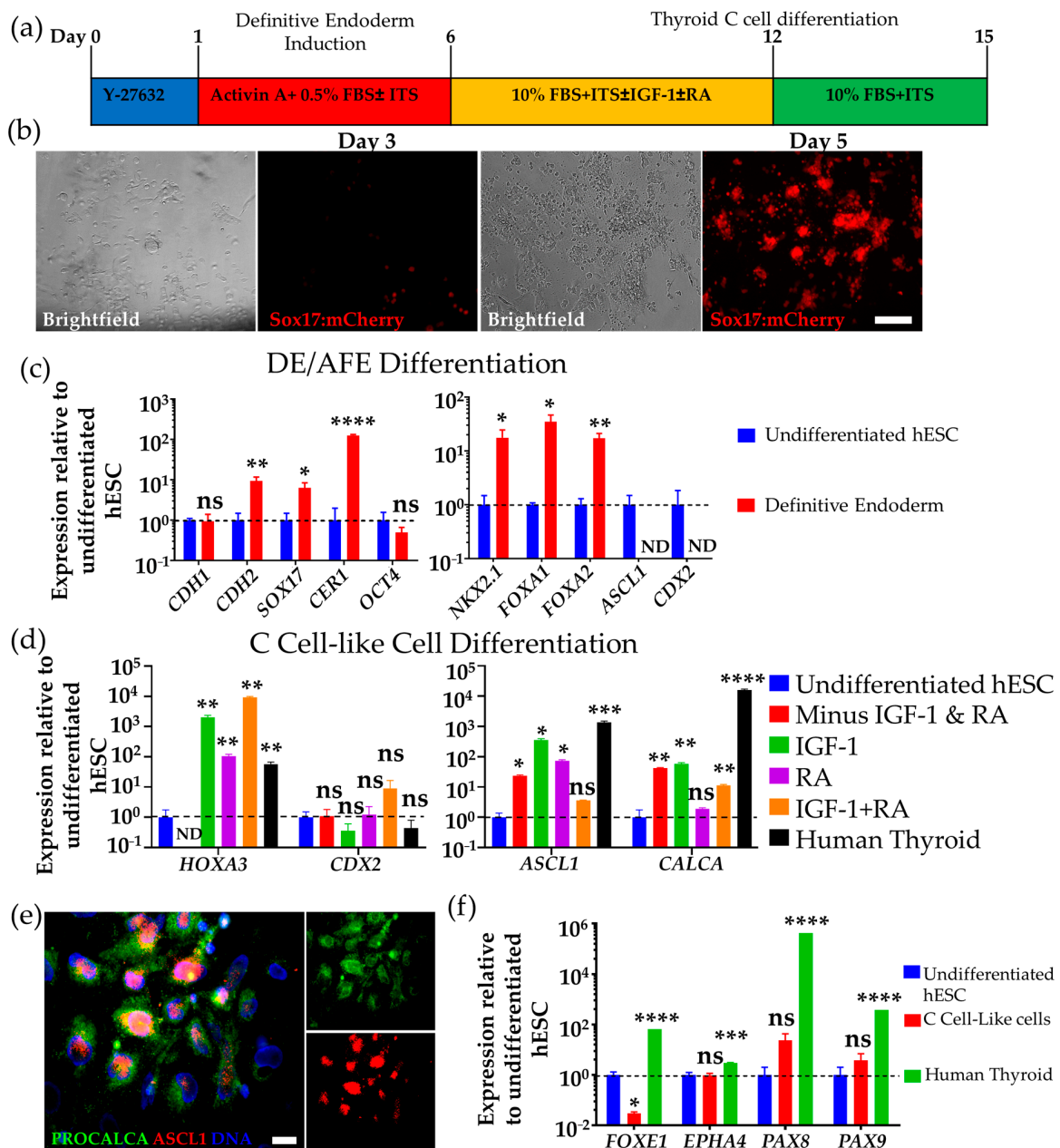


Figure 2. HESC-derived cells express definitive endoderm/anterior foregut endoderm (DE/AFE) and thyroid C cell markers. (a). Differentiation protocol of hESCs to DE/AFE-like cells and further to thyroid C cell-like cells. (b) Microscopy analysis of DE/AFE-like cells induced after 3 and 5 days exposure to activin A showing the expression of SOX17 detected by mCherry expression using the H9 hESC-SOX17 mCherry reporter line. Scale bar: 200 μ m. (c) qPCR analysis of DE/AFE-like cells at day 6 (red bars) normalized to undifferentiated hESC (blue bars), showing downregulation of pluripotency marker OCT4, no expression of posterior foregut marker CDX2, upregulation of diverse early DE/AFE markers, and no expression

of the later C cell marker *ASCL1*. (d) qPCR analysis of DE/AFE-like cells differentiated to thyroid C cell-like cells at day 15 normalized to undifferentiated hESC (blue bar) comparing different conditions (no IGF1 and no RA, red bar; IGF1 only, green bar; RA only, purple bar; IGF1 and RA, orange bar) with human thyroid (black bar) (commercial cDNA library). Consistent with thyroid C cell lineage is elevated expression of *ASCL1*, *HOXA3*, and *CALCA* and depression of *CDX2* (posterior foregut lineage). (e) Immunofluorescence of H9 hESC-derived DE/AFE-like cells differentiated with IGF-1 (day 15 of differentiation), showing co-expression of C cell lineage markers, *ASCL1* (red) and *PROCALCITONIN* (green). Scale bar: 50 μ m. (f) qPCR analysis of differentiated thyroid C cell-like cells differentiated with IGF-1 for 6 days (day 15 of differentiation; red bar) normalized to undifferentiated H9 hESC (blue bar) comparing the expression of thyroid follicular and C cell transcription factors. Human thyroid was used as a positive control (green bar). *FOXE1* is confined to the follicular lineage while *PAX8*, *PAX9*, and *EPHA4* are expressed in both lineages but only early and transiently in the C cell lineage. N.D., not detected; n.s., not significant, * $p < 0.05$, ** $p < 0.01$, *** $p < 0.001$, **** $p < 0.0001$. $n = 3$ independent experiments (H9 hESC). Error bars represent mean \pm SEM. Insulin-like Growth Factor 1 (IGF1); Retinoic acid (RA); definitive endoderm (DE); anterior foregut endoderm (AFE); human embryonic stem cells (hESC).

2.3. Thyroid C Cell Differentiation Using 3D Gel Matrigel Scaffold Cultures

hESCs were harvested as discussed above, and 1×10^5 cells were resuspended in 35% Matrigel (*v/v*) (Corning-In Vitro Technologies, Lane Cove West, Australia) in DMEM/F12 supplemented with 0.5% FBS and 1X ITS-A, and seeded into 2 wells of a 96 well plate (50,000 cells per well); then they were placed in the incubator 37 °C for 60 min for the gel to cast before we topped the well up with DMEM/F12 supplemented with 0.5% FBS, 1X ITS-A, and 100 ng/mL activin A and cultured them at 37 °C and 5% CO₂ in a humidified incubator. This was counted as day 1, and culture proceeded for 5 days. Medium change was done after 2 days and then every day. On day 6, medium was changed to DMEM/F12 supplemented with 10% FBS, 1X ITS-A, and 2 ng/mL IGF-1 for 6 days. Medium change was done every day until day 12, where the cells were cultured without IGF-1 for 3 days. On day 15, cells were stimulated with Ca²⁺ for calcitonin secretion before harvesting cells for RNA extraction.

2.4. Immunocytochemistry/Immunofluorescence

Cells, both 2D and 3D, were fixed with 4% paraformaldehyde (PFA) for 15 min at room temperature and washed three times with PBS. The cells were then permeabilised for 30 min with 0.2% Triton-X and 3% horse serum in PBS with 0.2% azide and further blocked with 1% horse serum in PBS-azide for 30 min. The cells were then washed once with PBS-azide and stained with primary antibodies per the manufacturer's instructions and incubated at 4 °C overnight. Antibodies are listed in Table S1. Cells were then washed three times with PBS with a 5 min interval between PBS changes. For detection, cells were incubated with appropriate fluorochrome-conjugated secondary antibodies for 2–3 h at room temperature (see Table S1). Residual secondary antibodies were removed, and the cells were washed twice with PBS before counterstaining the nuclei with 10 ng/mL 4',6-diamidino-2-phenylindole dihydrochloride, DAPI (Sigma-Aldrich). Cells were then mounted in antifade mounting medium (90% glycerol (pH 8) with 200 mM DABCO; Sigma-Aldrich) and viewed using a Zeiss LSM 780 (Carl-Zeiss-Strasse, Oberkochen, Germany) confocal microscope.

For confocal optical sections, 3D differentiated cells in Matrigel were fixed in 4% PFA for 1 h at room temperature and washed three times with PBS. Immunostaining was done as above.

For cryostat sections, 3D differentiated cells in Matrigel were fixed with 4% PFA for 1 h at room temperature and placed in 30% sucrose in CMF-PBS overnight. Cells were then embedded in Tissue Tek OCT Medium in Tissue Tek cryomoulds (ProSciTech, Thuringowa, Australia) and frozen in dry ice-cooled isopentane. Sections were cut using a Leica CM 1900 cryostat microtome and collected on Superfrost microscope slides (Biolab Scientific, Auckland, New Zealand) coated with poly-L-lysine. Slides were stained as above. See the Supplementary Materials for antibody lists.

False antibody binding was checked by using a first antibody not reactive with human antigens and by omitting first antibodies. Reactivity of other antibodies were checked by using a known target, human kidney organoids supplied by Professor Melissa Little and Dr. Jessica Vanslambrouck.

2.5. RNA Extraction and qPCR

Total RNA was extracted from cultured cells using TRIzol (Thermo Fisher Scientific) and purified lysate by acid-phenol chloroform and later recovered by isopropanol/ethanol precipitation. Before cDNA synthesis, extracted RNA was digested with DNaseI (Promega, Sydney, Australia) following the manufacturer's instructions to remove residual DNA and synthesized using the Bioline SensiFAST™ cDNA Synthesis Kit (BIO-65054, Bioline (Aust) Pty Ltd- Eveleigh, Australia). We used the Human Thyroid Total RNA (Takara Bio-sourced from Scientifix Pty Ltd, Clayton, Australia) as a positive control. Briefly, 30–100 ng total RNA was converted into cDNA following the manufacturer's directions. Reactions were performed using cDNA converted from 30–100 ng of RNA, 50 nM of each primer, and AccuPower® 2X GreenStar Master Mix Solution (Bioneer Pacific, Kew East, Australia) in a total volume of 10 µL. Primers for qPCR analysis are listed in Table S3. For Taqman Assay analysis, reactions were performed using cDNA converted from 30–100 ng of RNA, 1X of Taqman Probe, and GoTaq® Probe qPCR Master Mix Solution (Promega) in a total volume of 10 µL. All runs were in triplicate and more than 3 ($n \geq 3$) independent experiments. *GAPDH* housekeeping gene was used for data normalization when the relevant gene was undetectable in the control population. Cultured hESCs were used as a calibration standard and relative gene expression changes were calculated using the $2^{-\delta\delta t}$ method. See the Supplementary Materials for primer lists.

2.6. FACs Sorting and Analysis

To detect intracellular proteins, we fixed cells with 2% PFA for 10 min and permeabilised them with 0.1% Triton-X in 1% horse serum, blocked them with 1% horse serum, and incubated them with primary antibodies in blocking buffer at 4 °C overnight. After they were washed with CMF-PBS and centrifuged, the appropriate secondary antibodies were added for 1 h and the cells were washed with CMF-PBS, pelleted, and resuspended in CMF-PBS containing 2% FBS. The cells were then strained (40 µm mesh; BD Falcon, North Ryde, Australia) and events were acquired with BD FACs X-20 Fortessa (BD Biosciences, Frenchs Forest, Australia). Data was analysed using CellQuest (BD Biosciences) and FCS Express 4 Flow (Denovo Software, Glendale, CA, USA).

2.7. Calcitonin Production and Secretion

To determine whether hESC-derived thyroid C cells produce calcitonin, we homogenized cells generated from hESCs in 2D culture in 200 µL sonication buffer consisting of 50 mM Tris-HCl pH 7.5, 0.1% SDS, and 2% EDTA (Thermo Fisher Scientific). Qsonica sonicator (Qsonica, Newtown, CT, USA) was used to sonicate the cells on ice with 1 burst at 25% amplitude for 5–10 s. Sonicated lysate was centrifuged for 5 min at 10,000 rpm, and the supernatant was used to analyse calcitonin concentration by ELISA.

To determine whether hESC-derived thyroid C-like cells are capable of secreting calcitonin on Ca^{2+} challenge, we washed cells generated from hESCs in either 2D or 3D conditions three times with a Krebs–Ringer buffer containing 10 mM HEPES. Cells were incubated with a 100 mM CaCl_2 solution in magnesium-free PBS at 37 °C for 90 min. Supernatants were then collected and analysed for calcitonin as above, and the remaining cells were then collected for RNA extraction and qPCR analysis.

2.8. ELISA Assay

Calcitonin levels were measured using a Human Procalcitonin ELISA kit (Thermo Fisher Scientific) following the manufacturer's instructions. Briefly, all reagents, standards, and samples were brought to room temperature (18–25 °C) before use. Then, 100 µL of each

procalcitonin standard, and sonicated and centrifuged sample was added to the supplied wells (duplicates per sample), which were pre-coated with procalcitonin antibody. Wells were then covered and incubated for 2–3 h at room temperature with gentle shaking. The solution was discarded, and wells were washed 4 times with 1X Wash Buffer. After the last wash, the remaining Wash Buffer was removed by aspiration and blotting by inverting against clean paper towels. Then, 100 μ L of 1X prepared biotinylated antibody was added to each well, which were incubated for 1 h at room temperature with gentle shaking. The solution was discarded, and the wells were washed 4 times with 1X Wash Buffer. Then, 100 μ L of prepared streptavidin-HRP solution was added and incubated for 45 min at room temperature with gentle shaking. The solution was discarded, and wells were washed 4 times with 1X Wash Buffer followed by adding 100 μ L of TMB substrate to each well. The plates were incubated for 30 min at room temperature in the dark with gentle shaking, and the reaction was stopped by adding 50 μ L of the stop solution to each well. Absorbance was measured on an ELISA plate reader set at 450 nm. The calculation of results was done using the ELISA software analysis tool online (elisaanalysis.com accessed on 2 April and 7 May 2017). The amounts of calcitonin were normalized by measuring total intracellular protein using a BCA protein assay kit (PIERCE, Thermo Fisher Scientific) as described below.

2.9. BCA Protein Assay (PIERCE)

Briefly, 25 μ L of each standard or the sample were added in replicate into a microplate well (working range = 20–2000 μ g/mL) (Thermo Fisher Scientific). Then, 200 μ L of the sample was added to each well and mixed thoroughly on a plate shaker for 30 s. The plate was covered and incubated at 37 °C for 30 min. Plates were then cooled to RT before measuring the absorbance at 562 nm on a plate reader. We then subtracted the average 562 nm absorbance measurement of the blank standard replicates from the 562 nm measurements of all other individual standard and unknown sample replicates and prepared a standard curve by plotting the average blank-corrected 562 nm measurement for each BSA standard vs. its concentration in μ g/mL. The standard curve was used to determine the protein concentration of each unknown sample.

2.10. Statistical Analyses

Data were analysed by using one-way ANOVA (when analysing only one variable-gene expression) and unpaired *t*-test with Welch's correction. Values were expressed as mean \pm SEM. Changes were deemed significant if the *p*-value was <0.05. Statistical significance is indicated as follows: * *p* < 0.05, ** *p* < 0.01, and *** *p* < 0.001. Graphs were drawn using GraphPad Prism v7.

3. Results

3.1. Differentiation of hESCs to Definitive Endoderm and Anterior Foregut Endoderm-like Cells

Recent research has thrown light on the embryonic origin, development, and differentiation of mouse thyroid C cells *in vivo*, proving that C cells originate from foregut endodermal cells via the ubb [34]. We modified a previous published protocol on differentiation of definitive endoderm (DE) [39,40] by adding ITS-A to the media to support the growth of the cells in the presence of low FBS [26] (Figure 2a). Three different human pluripotent cell lines, H9 and HES3 hESCs, and 007 iPSCs, were used in our studies.

To confirm the efficiency of our DE differentiation from hESCs, we used the Sox17-mCherry H9 hESC reporter line, provided by Professor Andrew Elefanty and Professor Ed Stanley, and analysed the number of mCherry expressing cells after 3 and 5 days exposure to activin A. The fidelity of mCherry and SOX17 expression has been previously demonstrated [41]. We recorded about 30–40% of cells expressing mCherry after 3 days differentiation with almost all cells (\geq 90%) expressing mCherry after 5 days differentiation with this protocol (Figure 2b).

The induced cells were analysed at day 6 for the expression of vertebrate DE markers [42,43] *FOXA2*, *CER1*, *CDH2* (N-cadherin), and *SOX17* by qPCR, and we observed an

upregulation of these genes together with a downregulation of the pluripotency marker, *OCT4*, while *CDH1* (E-cadherin) was unchanged (Figure 2c). A robust increase in a gene expressed in the anterior foregut endoderm (AFE), *NKX2.1* (also known as thyroid transcription factor 1, *TTF1*) [26], and *FOXA1* [34], was also found. *CDX2* is a marker for posterior foregut identity, and through qPCR analysis, we found that *CDX2* mRNA expression was undetected in the cultures (Figure 2c and Figure S1a,b), consistent with an anterior foregut identity. A similar finding was reported by Wells' group [44], consistent with long exposure to activin A promoting anterior foregut over posterior identity. The expression of the proneuronal gene *ASCL1* in the hESC-derived DE could not be detected (Figure 2d). This suggests the progenitors are at an early stage of DE differentiation since *ASCL1* expression in mouse C cell development begins later at around E11.5 [45], equivalent to the fifth week (Carnegie stage 14) in human embryos.

3.2. Differentiation of Human DE/AFE-like Cells to Thyroid C Cell-like Cells

Next, we sought to differentiate these cells into thyroid C cell-like cells by modifying previously published protocols on lung, hepatocyte, and thyroid progenitor cell differentiation, which involves using FGF2 and BMP4, as well as Wnt and Sonic hedgehog (Shh) factors [26,46,47]. Although the ubb fuses with the thyroid primordium later during mammalian development (see Figure 1), we sought to disfavour the differentiation of thyroid and lung progenitors by increasing the time of activin A exposure and by omitting dexamethasone, BMP4, FGF2, and Wnt agonists which promote thyroid and lung differentiation [26,48]. FGF2 and BMP4 exposure of endodermal lineage cells also promotes the differentiation of hepatocytes and pancreatic cells [49,50], therefore further supporting the omission of both BMP4 and FGF2. Both Shh agonists and antagonists were also omitted from the differentiation method since ectopic expression of Shh favours intestinal lineage differentiation [51]. Furthermore, although the ubb and hence thyroid C cells fail to fuse with the thyroid primordium in *Shh*^{-/-} mice, their development and differentiation are not affected [52], suggesting Shh is not required.

Given the extraordinary similarity in transcriptional read-out between neural crest-derived neurons and enteroendocrine cells [45], we used factors such as IGF-1 that have been used in neuronal differentiation of stem cells [53,54], with the idea being that this might favour C cell-like neuroendocrine differentiation of cells already embarked on the DE/AFE pathway. We also used IGF-1 for the differentiation on the basis that IGF-1 activates the PI3K/Akt1 and Ras/MAPK signalling pathways [55], which have been associated with anterior foregut endoderm specification and epithelialisation [56]. Cell interaction with extracellular matrix (ECM) such as laminin and collagen IV interact with PI3K/Akt1 and Ras/MAPK signalling which play a role in the specification of foregut precursors, and inhibition of the PI3K/Akt1 pathway disrupts anterior DE specification [56,57], and therefore we used ECM substrates. In addition, retinoic acid (RA) was tested as it favours many neural differentiations [58], as well as being important in specification of the third and fourth pharyngeal pouches, the origin of the ubb [59].

We differentiated the DE cells in high FBS while supplementing the medium with IGF-1 and retinoic acid (RA) for 6 days and analysed them after 3 days (day 15 total differentiation) on Matrigel-coated surfaces [31,47] (Figure 2a). On the basis of a previously published protocol where primary embryonic C cells were cultured in 5% FBS and 1% chick embryo extract, we employed FBS only, but increased its concentration from 5% to 10% [60].

We assessed which condition will lead to an increased expression of *ASCL1* and *CALCA*. The pro-neural gene *ASCL1* plays an important but late role in the development and differentiation of C cells, and *ASCL1* mutant mice lack C cells, although the thyroid gland develops normally (Figure 2c) [45]. *CALCA* encodes not only calcitonin, which is specific for C cells, but also calcitonin gene-related peptide (CGRP) and katecalcin by alternative RNA splicing and cleavage of precursor proteins. The development and migration of the ubb also depend on the expression of the paralogs of *HOX3*—an example

is *HOXA3* [45,61]. We further analysed which condition will disfavour posterior foregut identity by analysing the expression of *CDX2* mRNA.

Culture with no addition of growth factors and with the addition of RA only had no effect on mRNA expression of the posterior foregut marker, *CDX2*. Cultured cells treated with IGF-1 led to a reduced expression of *CDX2* (Figure 2c,d) to a similar level to that recorded in the commercial human adult thyroid sample. IGF-1 treatment also led to an increase in *ASCL1* and *CALCA* as compared to the other conditions and a comparable level of *HOXA3* expression comparing it to both IGF-1- and RA-treated conditions. Combining IGF-1 and RA resulted in the overexpression of *CDX2* mRNA as analysed by qPCR (Figure 2d), suggesting a more posterior endodermal patterning. We then confirmed the expression of *ASCL1*, procalcitonin, E-cadherin, and CGRP by immunostaining (Figures 2e and S1c,d). We also immunostained with *Islet1*, which has been shown to be a C cell precursor marker (see Figure S1e) [62]. These results are in congruence with previously published findings of the role of IGF-1-activated pathways in thyroid C cell development [57].

Next, in addition to *ASCL1* and *CALCA*, we asked whether the differentiated cells after 6 days of IGF-1 exposure express *FOXE1*, *EPHA4*, *PAX8*, and *PAX9*, which are highly expressed in the human thyroid in spatiotemporally specific patterns (see Figure 1). The expression of *FOXE1* (also known as *TTF2*, thyroid transcription factor 2) [63] is regulated by the expression of *NKX2.1* and *PAX8*, and its expression downstream of *NKX2.1* and *PAX8* distinguishes thyroid follicular progenitors from non-follicular cells during development [51,64]. Thyroid progenitors are specified by the expression of *PAX8* with *EPHA4* during thyroid folliculogenesis [51]. They are expressed ubiquitously at E9.5 in the mouse pharyngeal endoderm [61] but the ubb begins to lose *EPHA4* expression after delamination from the pharyngeal pouch followed by complete loss of *EPHA4* expression when the ubb merges with the median thyroid *anlage* [65]. Expression of *PAX9* also plays an important role in the patterning of the pharyngeal pouches, as well as regulating calcitonin gene transcription [66,67]. To this end, we performed qPCR analyses on these genes which are expressed in human adult thyroid from a commercial cDNA library (see Table S2). The qPCR results show a comparable expression of markers between our differentiated cells and the human thyroid. Although there were higher fold differences in follicular markers *FOXE1*, *PAX8*, and *PAX9* expression in the human thyroid resource (which was derived from both follicular and parafollicular cells), there was no significant change in *EPHA4* expression in hESC-derived C cell-like cells relative to undifferentiated hESC (Figure 2f). The reduction in *FOXE1* mRNA expression is consistent with the development of C cells and also indicates that the differentiated cells are not follicular thyroid cells [51].

To investigate the efficiency of our differentiation protocol, we performed FACS analyses on the cells after 3 days of IGF-1 differentiation to examine expression of calcitonin, procalcitonin, and *TUJ1*. The results show that by day 3, approximately 9% of the cells expressed the procalcitonin marker, 6% expressed calcitonin, and more than 40% expressed *TUJ1*. C cells have been shown to express the neuronal marker *TUJ1* during early development at E14.5 in mouse [45,60,61]; therefore, taken together, the results support hESC differentiation towards a thyroid C cell-like lineage by this stage (Figure 3a). Analysis of day 15 differentiated cells by qPCR showed the expression of thyroid C cell markers *FOXA1*, *FOXA2*, *NKX2.1*, *RET*, and *CALCA* (Figure 3b, and refer to Figure 2d for *CALCA* expression). However, the expression of *SOX17* indicates the continued presence of undifferentiated endodermal progenitors (Figure 3b). We then immunostained for E-cadherin, procalcitonin, and CGRP; these are markers expressed by C cells with procalcitonin being restricted to the C cell lineage [14,31,45]. We show that more than 50% of the cells co-expressed E-cadherin and procalcitonin indicating that this differentiation protocol is generating thyroid C cell-like cells in vitro (Figure 4a,b). We performed qPCR analysis to further support that our differentiation protocol disfavors the differentiation of lung epithelial cells and the results showed the downregulation of lung epithelial cell specific genes, *SFTPC* and *CC10* (see Figure S2c). We further immunostained for thyroid follicular marker *PAX8* to investigate the efficiency of the differentiation protocol, and the negative

result indicated the absence of thyroid follicular cells. Staining on the positive control (kidney organoids) indicates the validity of this antibody (see Figure S3a,b).

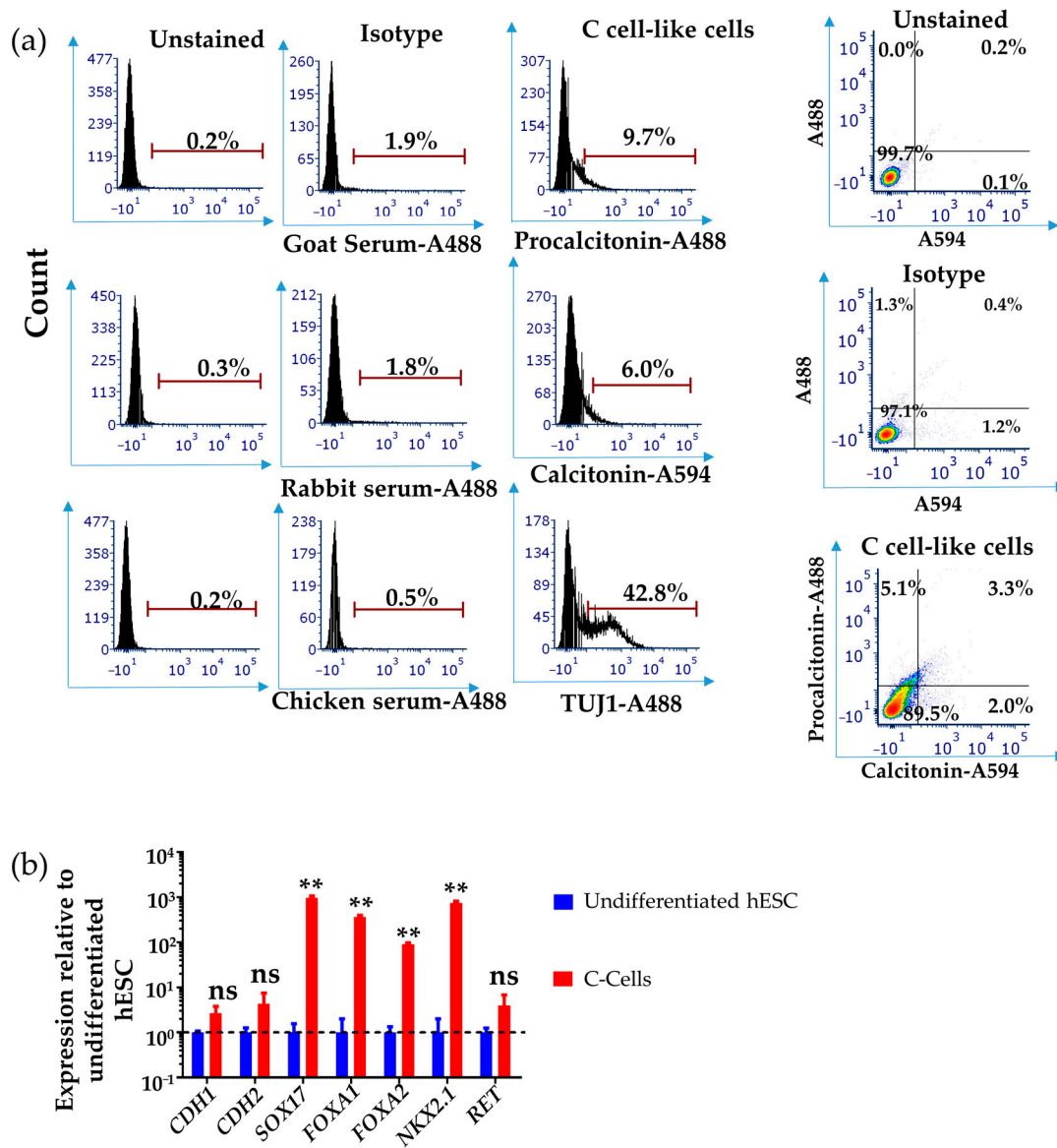


Figure 3. hESC-derived cells express thyroid C cell markers. (a) Representative FACS plots of H9 hESC-derived DE/AFE cells differentiated to thyroid C cell-like cells after 3 days of exposure to IGF-1 as analysed using PROCALCITONIN, CALCITONIN, and TUJ1 antibodies. The plot suggests emergence of PROCAL+/CALC+ sub-populations after 3 days of IGF-1 exposure while more than 40% of the cells express TUJ1, a neuronal marker expressed in C cells. (b) qPCR analysis of day 15 differentiated thyroid C cell-like cells (red bars) comparing the expression of C cell markers, normalised to undifferentiated hESC (H9, blue bars). Error bars represent mean \pm SEM. n.s., not significant, ** $p < 0.01$. $n = 3$ independent experiments. Human embryonic stem cells (hESC).

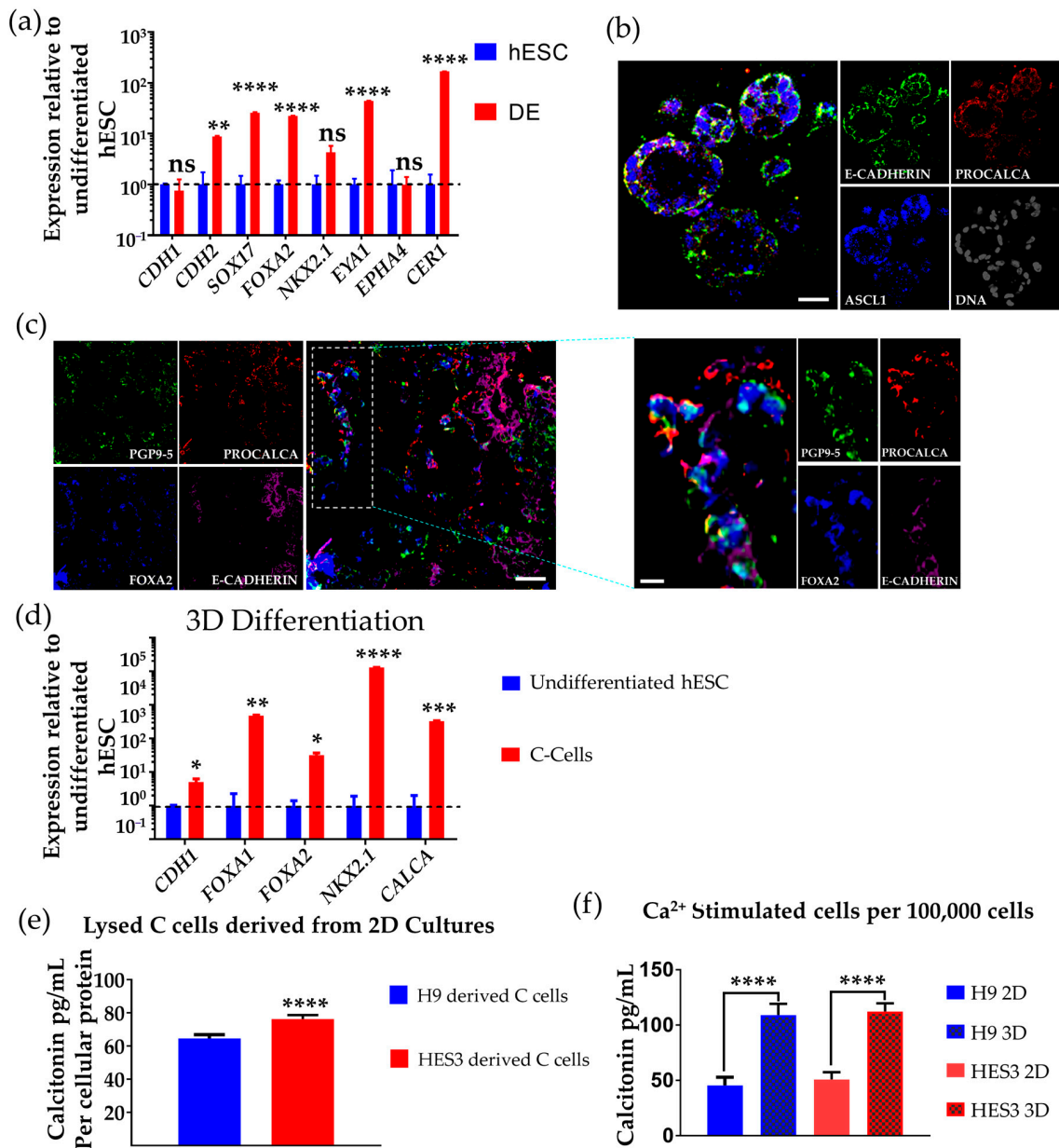


Figure 4. Differentiated human thyroid C cell-like cells produce calcitonin in culture. (a) qPCR analysis of 3D differentiation of DE/AFE-like cells (red bars) at day 6 normalized to undifferentiated hESC (blue bars), showing upregulation of DE/AFE markers. *n* = 3 independent experiments (H9 hESC). (b) Immunostained confocal optical section of day 15 H9 hESC differentiated thyroid C cell-like cells in 3D Matrigel culture co-expressing *E-CADHERIN* (green), *PROCALCITONIN* (red), and *ASCL1* (blue). Nuclei are shown in grey. Scale bar: 50 µm. (c) Immunofluorescence of cryosectioned H9 hESC differentiated thyroid C cell-like cells (day 15) in 3D Matrigel co-expressing *E-CADHERIN* (purple), *PROCALCITONIN* (red), *FOXA2* (blue), and *PGP9.5* (green). Scale bar: 100 µm. (d) qPCR analysis of 3D differentiation of C cell-like cells with IGF-1 (day 15 of differentiation) (red bars) normalised to undifferentiated hESC (H9, blue bars). *n* = 3 independent experiments. (e) ELISA analysis of differentiated thyroid C cell-like cells (H9 hESC-derived, blue bars; HES3 hESC-derived, red bars) at day 15 of 2D culture showing the production of calcitonin (cells lysed in 200 µL buffer) normalised to the total cellular protein as measured by BCA representing of 0.5–1 × 10⁶ cells. Error bars represent mean ± SEM. *n* = 3 independent experiments. (f) Comparison of the secretion of calcitonin by cells differentiated in the 2D (unpatterned bars) and 3D (patterned bars) format (day 15 of differentiation) into the medium (200 µL) as stimulated by 100 mM Ca²⁺ per 100,000 cells (H9 hESC-derived, blue bars; HES3 hESC-derived red bars). Error bars represent mean ± SEM. n.s., not significant, * *p* < 0.05, ** *p* < 0.01, *** *p* < 0.001, **** *p* < 0.0001. *n* = 3 independent experiments. Human embryonic stem cells (hESC); definitive endoderm (DE); anterior foregut endoderm (AFE).

3.3. Differentiation of hESCs to Neuroendocrine Thyroid C Cell-like Cells in 3D Matrigel

The interaction in vitro between ECM and cells regulates cell differentiation by providing a microenvironment mimicking that found in vivo, and this has been shown in vitro in neural differentiation [68], kidney differentiation [69], small intestine differentiation [70], colon differentiation [71], development of pancreatic beta islet cells [72], and development of thyroid follicular cells [73]. We hypothesised that differentiating hESCs to thyroid C cell-like cells in 3D format in ECM (as compared to 2D on ECM) will support more efficient generation of thyroid C cell-like cells and the production of calcitonin.

Dissociated hESCs were embedded in Matrigel and differentiation following the same protocol as for monolayer culture (see Figure 2a). At day 6, the cells were analysed by qPCR for the DE/AFE markers and showed expression of *SOX17*, *FOXA2*, *NKX2.1*, *CER1*, *EYA1*, and *CDH2* (Figure 2c). We then further differentiated the cells to C cell-like cells using the same IGF-1 protocol as with the monolayer cultures. We performed confocal optical section and cryosection analysis of 3D cultures for E-cadherin, procalcitonin, and ASCL1 and the neuroendocrine marker PGP9.5, and found co-expression at day 15 in more than 70% of the cells [31,61] (Figure 4b,c). It is noteworthy here that C cells can form follicle-like structures, and this has been shown to be its appearance of the ubb during development in some mammalian and non-mammalian species [28,74]. Immunostaining of 3D cultures also showed expression of E-cadherin, procalcitonin, PGP9.5, and *FOXA2*. Of particular importance for C cell differentiation is procalcitonin, as expression of this is restricted to later stages in the thyroid C cell lineage [14,31,34,45]. qPCR analysis of differentiated cells with IGF-1 in 2D culture (day 15 of differentiation) showed the expression of thyroid C cell markers *FOXA1*, *FOXA2*, *NKX2.1*, *RET*, and *CALCA* (Figure 3b, and refer to Figure 2d for *CALCA* expression). qPCR analysis of differentiated cells at equivalent time and in 3D culture showed the expression of C cell markers *FOXA1*, *FOXA2*, *NKX2.1*, and *CALCA* (Figure 4d).

3.4. Determination of Calcitonin Production and Secretion on Ca^{2+} Challenge

The distinctive function of thyroid C cells is the production of calcitonin, a hormone that regulates Ca^{2+} metabolism by lowering blood Ca^{2+} levels. To assess the potential functionality of the hESC-derived C cell-like cells, we first had to confirm whether these cells were producing calcitonin, and to that end, cells were lysed in 0.2 mL of lysis buffer after 15 days differentiation in 2D conditions and analysed by ELISA. The ELISA results were then normalised to the total cellular protein analysed by BCA assay. The results showed that the cells were producing 12.8 to 20.2 pg (64–101 pg/mL in a volume of 200 μ L culture medium) of calcitonin per $0.5\text{--}1 \times 10^6$ cells with the cells derived from HES3 cell line at 76.3 pg/mL (15.3 pg of calcitonin per $0.5\text{--}1 \times 10^6$ cells) and the H9 hESC cell line at 64.5 pg/mL (12.9 pg of calcitonin per $0.5\text{--}1 \times 10^6$ cells) (Figure 4e).

We then investigated whether the cells were capable of secreting calcitonin into the medium when challenged with Ca^{2+} by adding calcium chloride (final concentration of 100 mM) to the cells. Assessment of the supernatant by ELISA showed calcitonin secretion from the differentiated C cell-like cells after 15 days differentiation (Figure 4f). We detected calcitonin secretion of 109 and 112 pg/mL (21.8 and 22.4 pg per calcitonin per 1×10^5 cells) from induced C cell-like cells in 3D, which represented a 2.4- and 2.2-fold increase in calcitonin secretion compared to that detected in cells from parallel 2D-induced cultures of H9 and HES3 hESCs, respectively (Figure 4f). Comparing the number of cells producing calcitonin in culture as measured by ELISA, $0.5\text{--}1 \times 10^6$ cells in 2D against 1×10^5 in 3D, we were able to infer that the number of cells producing calcitonin in 3D was approximately two times more than that in the 2D format. Thus, per every 10,000 cells, H9 hESC differentiated C cells released between 0.13–6.45 pg of calcitonin in the 2D format and 2.18–10.9 pg of calcitonin in 3D. This also further supports the idea that the cell or tissue differentiation is more efficient in a 3D format relative to 2D [75].

4. Discussion

Difference in the immune system, physiology, individual genetic backgrounds, and other factors makes the use of animals and animal cells as models for the study of the pathophysiology of many human diseases inadequate [22]. As a result of this, much attention has been directed recently to disease modelling using human pluripotent stem cells. Here, we have developed a novel protocol that allows for the generation of functional parafollicular cells (thyroid C cell-like cells) from hESCs. This complements a method for producing thyroid follicular-like cells from human pluripotent cells [26,64]. Combining the two induced lineages offers the potential to form a complete thyroid complement of cells.

Our results demonstrate the directed differentiation of hESC into DE cells and then AFE progenitors with thyroid C cell differentiation potential. The main objective of this protocol was to look for factors that will disfavour the differentiation of other cell lineages from the AFE and at the same time favour the differentiation of thyroid C cell-like cells expressing the required markers. The DE/thyroid C cell-like cell differentiation method was robust with little variability across three pluripotent cell lines (H9 and HES3 hESCs and 007 iPSCs) in the generation of calcitonin producing cells as assayed by PCR, immunolabelling, and ELISA.

To provide a temporally and spatially controlled environment which preferentially supports stem cell differentiation and maturation, researchers have used ECM-like collagen and Matrigel [72,76]. Here, we demonstrated the feasibility of differentiating thyroid C cells from hESCs using Matrigel as ECM. These 3D cultured cells produced and, on Ca^{2+} stimulation, released more calcitonin as analysed by ELISA than the cells in 2D culture, which was similar to previous findings that ECM supports stem cell differentiation and maturation [36,37,75,76].

In conclusion, these human thyroid C cell-like cells derived from pluripotent cells have the potential for investigating the pathogenesis and modelling of MTC and provide a platform for the screening of combinatorial drugs.

Supplementary Materials: The following are available online at <https://www.mdpi.com/article/10.3390/cells10112897/s1>, Figure S1: (a) QPCR analysis of DE/AFE-like cells normalized to undifferentiated hiPSC (007 cell line), showing time course upregulation of SOX17. No significant difference was recorded. N.D., not detected. $n = 3$ independent experiments. Error bars represent mean \pm SEM. (b) QPCR analysis of DE/AFE-like cells normalized to undifferentiated hiPSC (007 cell line) and hESC (HES3), showing time course upregulation of NKX2.1. No significant difference was recorded. N.D., not detected. $n = 3$ independent experiments. Error bars represent mean \pm SEM. (c) Immunofluorescence of differentiated thyroid C cell-like cells grown on laminin showing co-expression of C cell lineage markers, E-CADHERIN, CGRP, and PROCALCITONIN. Scale bar: 100 μm . (d) Immunofluorescence of differentiated thyroid C cell-like cells grown on Matrigel showing co-expression of C cell lineage markers, E-CADHERIN, CGRP, and PROCALCITONIN. Scale bar: 20 μm . (e) Immunofluorescence of differentiated thyroid C cell-like cells grown on Matrigel showing co-expression of C cell lineage markers, E-CADHERIN, ISL1, and PROCALCITONIN. Scale bar: 20 μm . Figure S2: (a) Wholemout staining of differentiated thyroid C cell-like cells in 3D Matrigel culture co-expressing E-CADHERIN, PROCALCITONIN, and ASCL1. Scale bar: 100 μm . (b) Wholemout staining of differentiated thyroid C cell-like cells in 3D matrigel co-expressing PGP9.5, E-CADHERIN, and CALCITONIN. Scale bar: 100 μm . (c) QPCR analysis of thyroid C cell-like cells normalized to differentiated DE/AFE (007 cell line), showing the downregulation of lung markers CC10 and SFTPC and upregulation of thyroid C cell-like cell, CALCA. No significant difference was recorded. N.D., not detected. $n = 3$ independent experiments. Error bars represent mean \pm SEM. Figure S3: (a) Immunofluorescence of differentiated thyroid C cell-like cells grown on Laminin showing co-expression of C cell lineage markers NKX2.1 and PROCALCITONIN, and no expression of thyroid marker PAX8. Scale bar: 200 μm (upper) and 100 μm (lower). (b) Immunofluorescence of differentiated kidney cells as a positive control showing the specificity of the PAX8 antibody. Scale bar: 200 μm (upper) and 100 μm (lower). Table S1: Table of antibodies; Table S2: qPCR probes; Table S3: PCR primers for SYBR gene qPCR.

Author Contributions: K.D.A.-B. designed and performed the in vitro experiments. K.D.A.-B. and D.F.N. wrote the manuscript. K.D.A.-B., M.D. and D.F.N. approved the final draft of the manuscript. M.D. and D.F.N. provided the funding for this project. All authors have read and agreed to the published version of the manuscript.

Funding: This research was supported by NHMRC grant 1069757, grant 1050692, Stem Cells Australia SCA 2013F-9, Australian Research Council Future Fellowship FT130100514 (M.D.), The University of Melbourne, and Murdoch Children’s Research Institute, MCRI. K.D.A.-B. was funded by an IPRS and APA (Int) PhD Scholarship through the Department of Paediatrics, University of Melbourne.

Institutional Review Board Statement: All experiments were performed with the approval from the Murdoch Children’s Research Institute Institutional Biosafety Committee 226-2015 PC2. The study was conducted according to the guidelines of the Declaration of Helsinki, and approved by the University of Melbourne Human Ethics, ID 1545384, 0605017 and 1545394.

Informed Consent Statement: Consent was not needed for this specific research as the hESC lines were purchased from companies or provided by collaborators, which were all generated with patient consent to distribute the cell lines to other researchers for research purposes.

Data Availability Statement: The study did not report any data.

Acknowledgments: We acknowledge the Victorian Government’s Operational Infrastructure Support Program to Murdoch Children’s Research Institute, MCRI. We thank Andrew Elefanty and Ed Stanley for providing the Sox17-mCherry cell line, Alice Pébay for providing the 007 iPSC cell line and Melissa Little and Jessica Vanslambrouck for providing the kidney organoid. We also thank Matthew Burton and Paul Lau (Flow Cytometry-MCRI) for their technical advice and support.

Conflicts of Interest: The authors declare no conflict of interest.

References

1. Nikiforov, Y.E. Thyroid carcinoma: Molecular pathways and therapeutic targets. *Mod. Pathol.* **2008**, *21* (Suppl. 2), S37–S43. [[CrossRef](#)]
2. Lin, R.Y. Thyroid cancer stem cells. *Nat. Rev. Endocrinol.* **2011**, *7*, 609–616. [[CrossRef](#)] [[PubMed](#)]
3. Hundahl, S.A.; Fleming, I.D.; Fremgen, A.M.; Menck, H.R. A National Cancer Data Base report on 53,856 cases of thyroid carcinoma treated in the U.S., 1985–1995 [see comments]. *Cancer* **1998**, *83*, 2638–2648. [[CrossRef](#)]
4. Davies, L.; Welch, H.G. Increasing incidence of thyroid cancer in the United States, 1973–2002. *JAMA* **2006**, *295*, 2164–2167. [[CrossRef](#)] [[PubMed](#)]
5. Siegel, R.L.; Miller, K.D.; Jemal, A. Cancer statistics, 2018. *CA Cancer J. Clin.* **2018**, *68*, 7–30. [[CrossRef](#)] [[PubMed](#)]
6. Siegel, R.L.; Miller, K.D.; Jemal, A. Cancer statistics, 2019. *CA Cancer J. Clin.* **2019**, *69*, 7–34. [[CrossRef](#)]
7. Vergamini, L.B.; Frazier, A.L.; Abrantes, F.L.; Ribeiro, K.B.; Rodriguez-Galindo, C. Increase in the incidence of differentiated thyroid carcinoma in children, adolescents, and young adults: A population-based study. *J. Pediatr.* **2014**, *164*, 1481–1485. [[CrossRef](#)]
8. Chen, A.Y.; Jemal, A.; Ward, E.M. Increasing incidence of differentiated thyroid cancer in the United States, 1988–2005. *Cancer* **2009**, *115*, 3801–3807. [[CrossRef](#)]
9. Wells, S.A., Jr.; Pacini, F.; Robinson, B.G.; Santoro, M. Multiple endocrine neoplasia type 2 and familial medullary thyroid carcinoma: An update. *J. Clin. Endocrinol. Metab.* **2013**, *98*, 3149–3164. [[CrossRef](#)]
10. Vaclavikova, E.; Kavalcova, L.; Skaba, R.; Dvorakova, S.; Macokova, P.; Rouskova, B.; Bendlova, B. Hirschsprung’s disease and medullary thyroid carcinoma: 15-year experience with molecular genetic screening of the RET proto-oncogene. *Pediatric Surg. Int.* **2012**, *28*, 123–128. [[CrossRef](#)]
11. Waguespack, S.G.; Rich, T.A.; Perrier, N.D.; Jimenez, C.; Cote, G.J. Management of medullary thyroid carcinoma and MEN2 syndromes in childhood. *Nat. Rev. Endocrinol.* **2011**, *7*, 596–607. [[CrossRef](#)]
12. Roy, M.; Chen, H.; Sippel, R.S. Current understanding and management of medullary thyroid cancer. *Oncologist* **2013**, *18*, 1093–1100. [[CrossRef](#)]
13. Frendo, J.L.; Delage-Mourroux, R.; Cohen, R.; Pichaud, F.; Pidoux, E.; Guliana, J.M.; Jullienne, A. Calcitonin receptor mRNA expression in TT cells: Effect of dexamethasone. *Mol. Cell. Endocrinol.* **1998**, *139*, 37–43. [[CrossRef](#)]
14. Hazard, J.B. The C cells (parafollicular cells) of the thyroid gland and medullary thyroid carcinoma. A review. *Am. J. Pathol.* **1977**, *88*, 213–250.
15. Dionigi, G.; Bianchi, V.; Rovera, F.; Boni, L.; Piantanida, E.; Tanda, M.L.; Dionigi, R.; Bartalena, L. Medullary thyroid carcinoma: Surgical treatment advances. *Expert Rev. Anticancer Ther.* **2007**, *7*, 877–885. [[CrossRef](#)]
16. Dionigi, G.; Tanda, M.L.; Piantanida, E. Medullary thyroid carcinoma: Surgical treatment advances. *Curr. Opin. Otolaryngol. Head Neck Surg.* **2008**, *16*, 158–162. [[CrossRef](#)]

17. Perez, C.A.; Arango, B.A.; Velez, M.; Raez, L.E.; Santos, E.S. Emerging role of multikinase inhibitors for refractory thyroid cancer. *Biologics* **2012**, *6*, 257–265. [[CrossRef](#)]
18. Mologni, L.; Gambacorti-Passerini, C.; Goekjian, P.; Scapozza, L. RET kinase inhibitors: A review of recent patents (2012–2015). *Expert Opin. Ther. Pat.* **2017**, *27*, 91–99. [[CrossRef](#)] [[PubMed](#)]
19. Colman, A.; Dreesen, O. Pluripotent stem cells and disease modeling. *Cell Stem Cell* **2009**, *5*, 244–247. [[CrossRef](#)]
20. Gingold, J.; Zhou, R.; Lemischka, I.R.; Lee, D.F. Modeling Cancer with Pluripotent Stem Cells. *Trends Cancer* **2016**, *2*, 485–494. [[CrossRef](#)] [[PubMed](#)]
21. Lee, D.F.; Su, J.; Kim, H.S.; Chang, B.; Papatsenko, D.; Zhao, R.; Yuan, Y.; Gingold, J.; Xia, W.; Darr, H.; et al. Modeling familial cancer with induced pluripotent stem cells. *Cell* **2015**, *161*, 240–254. [[CrossRef](#)]
22. Passier, R.; Orlova, V.; Mummery, C. Complex Tissue and Disease Modeling using hiPSCs. *Cell Stem Cell* **2016**, *18*, 309–321. [[CrossRef](#)] [[PubMed](#)]
23. Dye, B.R.; Hill, D.R.; Ferguson, M.A.; Tsai, Y.H.; Nagy, M.S.; Dyal, R.; Wells, J.M.; Mayhew, C.N.; Nattiv, R.; Klein, O.D.; et al. In vitro generation of human pluripotent stem cell derived lung organoids. *eLife* **2015**, *4*. [[CrossRef](#)] [[PubMed](#)]
24. Parent, A.V.; Russ, H.A.; Khan, I.S.; LaFlam, T.N.; Metzger, T.C.; Anderson, M.S.; Hebrok, M. Generation of functional thymic epithelium from human embryonic stem cells that supports host T cell development. *Cell Stem Cell* **2013**, *13*, 219–229. [[CrossRef](#)]
25. Dame, K.; Cincotta, S.; Lang, A.H.; Sanghrajka, R.M.; Zhang, L.; Choi, J.; Kwok, L.; Wilson, T.; Kandula, M.M.; Monti, S.; et al. Thyroid Progenitors Are Robustly Derived from Embryonic Stem Cells through Transient, Developmental Stage-Specific Overexpression of Nkx2-1. *Stem Cell Rep.* **2017**, *8*, 216–225. [[CrossRef](#)] [[PubMed](#)]
26. Longmire, T.A.; Ikonomidou, L.; Hawkins, F.; Christodoulou, C.; Cao, Y.; Jean, J.C.; Kwok, L.W.; Mou, H.; Rajagopal, J.; Shen, S.S.; et al. Efficient derivation of purified lung and thyroid progenitors from embryonic stem cells. *Cell Stem Cell* **2012**, *10*, 398–411. [[CrossRef](#)]
27. Fagman, H.; Nilsson, M. Morphogenesis of the thyroid gland. *Mol. Cell. Endocrinol.* **2010**, *323*, 35–54. [[CrossRef](#)] [[PubMed](#)]
28. Kusakabe, T.; Hoshi, N.; Kimura, S. Origin of the ultimobranchial body cyst: T/ebp/Nkx2.1 expression is required for development and fusion of the ultimobranchial body to the thyroid. *Dev. Dyn.* **2006**, *235*, 1300–1309. [[CrossRef](#)]
29. Kameda, Y.; Nishimaki, T.; Chisaka, O.; Iseki, S.; Sucov, H.M. Expression of the epithelial marker E-cadherin by thyroid C cells and their precursors during murine development. *J. Histochem. Cytochem. Off. J. Histochem. Soc.* **2007**, *55*, 1075–1088. [[CrossRef](#)]
30. Cote, G.J.; Grubbs, E.G.; Hofmann, M.C. Thyroid C-Cell Biology and Oncogenic Transformation. *Recent Results Cancer Res.* **2015**, *204*, 1–39. [[CrossRef](#)]
31. Kameda, Y. Morphological and molecular evolution of the ultimobranchial gland of nonmammalian vertebrates, with special reference to the chicken C cells. *Dev. Dyn. Off. Publ. Am. Assoc. Anat.* **2017**, *246*, 719–739. [[CrossRef](#)] [[PubMed](#)]
32. Le Douarin, N.; Fontaine, J.; Le Lievre, C. New studies on the neural crest origin of the avian ultimobranchial glandular cells—interspecific combinations and cytochemical characterization of C cells based on the uptake of biogenic amine precursors. *Histochemistry* **1974**, *38*, 297–305. [[CrossRef](#)]
33. Zabel, M. Parafollicular cells of the rat thyroid gland after treatment with vitamin D. *Acta Anat. (Basel)* **1984**, *118*, 18–22. [[CrossRef](#)] [[PubMed](#)]
34. Johansson, E.; Andersson, L.; Ornros, J.; Carlsson, T.; Ingeson-Carlsson, C.; Liang, S.; Dahlberg, J.; Jansson, S.; Parrillo, L.; Zoppoli, P.; et al. Revising the embryonic origin of thyroid C cells in mice and humans. *Development* **2015**, *142*, 3519–3528. [[CrossRef](#)]
35. Dutta, D.; Heo, I.; Clevers, H. Disease Modeling in Stem Cell-Derived 3D Organoid Systems. *Trends Mol. Med.* **2017**, *23*, 393–410. [[CrossRef](#)]
36. Fitzgerald, A.A.; Li, E.; Weiner, L.M. 3D Culture Systems for Exploring Cancer Immunology. *Cancers* **2020**, *13*, 56. [[CrossRef](#)] [[PubMed](#)]
37. Krokker, L.; Szabo, B.; Nemeth, K.; Tohati, R.; Sarkadi, B.; Meszaros, K.; Patocs, A.; Butz, H. Three Dimensional Cell Culturing for Modeling Adrenal and Pituitary Tumors. *Pathol. Oncol. Res.* **2021**, *27*, 640676. [[CrossRef](#)]
38. Fagman, H.; Amendola, E.; Parrillo, L.; Zoppoli, P.; Marotta, P.; Scarfo, M.; De Luca, P.; de Carvalho, D.P.; Ceccarelli, M.; De Felice, M.; et al. Gene expression profiling at early organogenesis reveals both common and diverse mechanisms in foregut patterning. *Dev. Biol.* **2011**, *359*, 163–175. [[CrossRef](#)] [[PubMed](#)]
39. D’Amour, K.A.; Agulnick, A.D.; Eliazer, S.; Kelly, O.G.; Kroon, E.; Baetge, E.E. Efficient differentiation of human embryonic stem cells to definitive endoderm. *Nat. Biotechnol.* **2005**, *23*, 1534–1541. [[CrossRef](#)]
40. Kumar, N.; Brafman, D.; Willert, K. Endoderm Differentiation from Human Pluripotent Stem Cells. In *Working with Stem Cells*; Springer International Publishing: Cham, Switzerland, 2016; pp. 237–255. [[CrossRef](#)]
41. Loh, K.M.; Ang, L.T.; Zhang, J.; Kumar, V.; Ang, J.; Auyeong, J.Q.; Lee, K.L.; Choo, S.H.; Lim, C.Y.; Nichane, M.; et al. Efficient endoderm induction from human pluripotent stem cells by logically directing signals controlling lineage bifurcations. *Cell Stem Cell* **2014**, *14*, 237–252. [[CrossRef](#)]
42. Ang, S.L.; Wierda, A.; Wong, D.; Stevens, K.A.; Cascio, S.; Rossant, J.; Zaret, K.S. The formation and maintenance of the definitive endoderm lineage in the mouse: Involvement of HNF3/forkhead proteins. *Development* **1993**, *119*, 1301–1315. [[CrossRef](#)] [[PubMed](#)]
43. Kanai-Azuma, M.; Kanai, Y.; Gad, J.M.; Tajima, Y.; Taya, C.; Kurohmaru, M.; Sanai, Y.; Yonekawa, H.; Yazaki, K.; Tam, P.P.; et al. Depletion of definitive gut endoderm in Sox17-null mutant mice. *Development* **2002**, *129*, 2367–2379. [[CrossRef](#)] [[PubMed](#)]

44. Spence, J.R.; Mayhew, C.N.; Rankin, S.A.; Kuhar, M.F.; Vallance, J.E.; Tolle, K.; Hoskins, E.E.; Kalinichenko, V.V.; Wells, S.I.; Zorn, A.M.; et al. Directed differentiation of human pluripotent stem cells into intestinal tissue in vitro. *Nature* **2011**, *470*, 105–109. [[CrossRef](#)] [[PubMed](#)]
45. Kameda, Y.; Nishimaki, T.; Miura, M.; Jiang, S.X.; Guillemot, F. Mash1 regulates the development of C cells in mouse thyroid glands. *Dev. Dyn. Off. Publ. Am. Assoc. Anat.* **2007**, *236*, 262–270. [[CrossRef](#)]
46. Kadzik, R.S.; Morrisey, E.E. Directing lung endoderm differentiation in pluripotent stem cells. *Cell Stem Cell* **2012**, *10*, 355–361. [[CrossRef](#)]
47. Nilsson, M.; Fagman, H. Development of the thyroid gland. *Development* **2017**, *144*, 2123–2140. [[CrossRef](#)]
48. Goss, A.M.; Tian, Y.; Tsukiyama, T.; Cohen, E.D.; Zhou, D.; Lu, M.M.; Yamaguchi, T.P.; Morrisey, E.E. Wnt2/2b and beta-catenin signaling are necessary and sufficient to specify lung progenitors in the foregut. *Dev. Cell* **2009**, *17*, 290–298. [[CrossRef](#)]
49. Gouon-Evans, V.; Boussemart, L.; Gadue, P.; Nierhoff, D.; Koehler, C.I.; Kubo, A.; Shafritz, D.A.; Keller, G. BMP-4 is required for hepatic specification of mouse embryonic stem cell-derived definitive endoderm. *Nat. Biotechnol.* **2006**, *24*, 1402–1411. [[CrossRef](#)]
50. Xu, X.; Browning, V.L.; Odorico, J.S. Activin, BMP and FGF pathways cooperate to promote endoderm and pancreatic lineage cell differentiation from human embryonic stem cells. *Mech. Dev.* **2011**, *128*, 412–427. [[CrossRef](#)]
51. Nilsson, M.; Fagman, H. Mechanisms of thyroid development and dysgenesis: An analysis based on developmental stages and concurrent embryonic anatomy. *Curr. Top. Dev. Biol.* **2013**, *106*, 123–170. [[CrossRef](#)]
52. Westerlund, J. Misguided Migration of C Cell Precursors to Extra-Thyroidal Locations Related to Defective Pharyngeal Pouch Development in Shh Deficient Mice. *Cell Dev. Biol.* **2013**, *2*, 129. [[CrossRef](#)]
53. Brooker, G.J.; Kalloniatis, M.; Russo, V.C.; Murphy, M.; Werther, G.A.; Bartlett, P.F. Endogenous IGF-1 regulates the neuronal differentiation of adult stem cells. *J. Neurosci. Res.* **2000**, *59*, 332–341. [[CrossRef](#)]
54. Nieto-Estevez, V.; Defterali, C.; Vicario-Abejon, C. IGF-I: A Key Growth Factor that Regulates Neurogenesis and Synaptogenesis from Embryonic to Adult Stages of the Brain. *Front. Neurosci.* **2016**, *10*, 52. [[CrossRef](#)] [[PubMed](#)]
55. Laurino, L.; Wang, X.X.; de la Houssaye, B.A.; Sosa, L.; Dupraz, S.; Caceres, A.; Pfenninger, K.H.; Quiroga, S. PI3K activation by IGF-1 is essential for the regulation of membrane expansion at the nerve growth cone. *J. Cell Sci.* **2005**, *118*, 3653–3662. [[CrossRef](#)] [[PubMed](#)]
56. Villegas, S.N.; Rothova, M.; Barrios-Llerena, M.E.; Pulina, M.; Hadjantonakis, A.K.; Le Bihan, T.; Astrof, S.; Brickman, J.M. PI3K/Akt1 signalling specifies foregut precursors by generating regionalized extra-cellular matrix. *Elife* **2013**, *2*, e00806. [[CrossRef](#)] [[PubMed](#)]
57. Smedberg, J.L.; Smith, E.R.; Capo-Chichi, C.D.; Frolov, A.; Yang, D.H.; Godwin, A.K.; Xu, X.X. Ras/MAPK pathway confers basement membrane dependence upon endoderm differentiation of embryonic carcinoma cells. *J. Biol. Chem.* **2002**, *277*, 40911–40918. [[CrossRef](#)]
58. Gajovic, S.; St-Onge, L.; Yokota, Y.; Gruss, P. Retinoic acid mediates Pax6 expression during in vitro differentiation of embryonic stem cells. *Differentiation* **1997**, *62*, 187–192. [[CrossRef](#)] [[PubMed](#)]
59. Wendling, O.; Dennefeld, C.; Chambon, P.; Mark, M. Retinoid signaling is essential for patterning the endoderm of the third and fourth pharyngeal arches. *Development* **2000**, *127*, 1553–1562. [[CrossRef](#)]
60. Miura, M.; Kameda, Y. Neuronal properties in cultured ultimobranchial C cells of chick embryos: Process outgrowth and expression of TuJ1 and enkephalin. *Brain Res.* **2001**, *905*, 1–11. [[CrossRef](#)]
61. Kameda, Y. Cellular and molecular events on the development of mammalian thyroid C cells. *Dev. Dyn. Off. Publ. Am. Assoc. Anat.* **2016**, *245*, 323–341. [[CrossRef](#)]
62. Westerlund, J.; Andersson, L.; Carlsson, T.; Zoppoli, P.; Fagman, H.; Nilsson, M. Expression of Islet1 in thyroid development related to budding, migration, and fusion of primordia. *Dev. Dyn.* **2008**, *237*, 3820–3829. [[CrossRef](#)]
63. Kimura, S. Thyroid-specific transcription factors and their roles in thyroid cancer. *J. Thyroid. Res.* **2011**, *2011*, 710213. [[CrossRef](#)] [[PubMed](#)]
64. Ma, R.; Morshed, S.A.; Latif, R.; Davies, T.F. Thyroid cell differentiation from murine induced pluripotent stem cells. *Front. Endocrinol. (Lausanne)* **2015**, *6*, 56. [[CrossRef](#)]
65. Andersson, L.; Westerlund, J.; Liang, S.; Carlsson, T.; Amendola, E.; Fagman, H.; Nilsson, M. Role of EphA4 Receptor Signaling in Thyroid Development: Regulation of Folliculogenesis and Propagation of the C-Cell Lineage. *Endocrinology* **2011**, *152*, 1154–1164. [[CrossRef](#)] [[PubMed](#)]
66. Suzuki, M.; Katagiri, N.; Ueda, M.; Tanaka, S. Functional analysis of Nkx2.1 and Pax9 for calcitonin gene transcription. *Gen. Comp. Endocrinol.* **2007**, *152*, 259–266. [[CrossRef](#)] [[PubMed](#)]
67. Peters, H.; Neubuser, A.; Kratochwil, K.; Balling, R. Pax9-deficient mice lack pharyngeal pouch derivatives and teeth and exhibit craniofacial and limb abnormalities. *Genes Dev.* **1998**, *12*, 2735–2747. [[CrossRef](#)]
68. Philp, D.; Chen, S.S.; Fitzgerald, W.; Orenstein, J.; Margolis, L.; Kleinman, H.K. Complex extracellular matrices promote tissue-specific stem cell differentiation. *Stem Cells* **2005**, *23*, 288–296. [[CrossRef](#)]
69. Takasato, M.; Er, P.X.; Chiu, H.S.; Little, M.H. Generation of kidney organoids from human pluripotent stem cells. *Nat. Protoc.* **2016**, *11*, 1681–1692. [[CrossRef](#)]
70. Watson, C.L.; Mahe, M.M.; Munera, J.; Howell, J.C.; Sundaram, N.; Poling, H.M.; Schweitzer, J.I.; Vallance, J.E.; Mayhew, C.N.; Sun, Y.; et al. An in vivo model of human small intestine using pluripotent stem cells. *Nat. Med.* **2014**, *20*, 1310–1314. [[CrossRef](#)]

71. Munera, J.O.; Sundaram, N.; Rankin, S.A.; Hill, D.; Watson, C.; Mahe, M.; Vallance, J.E.; Shroyer, N.F.; Sinagoga, K.L.; Zarzoso-Lacoste, A.; et al. Differentiation of Human Pluripotent Stem Cells into Colonic Organoids via Transient Activation of BMP Signaling. *Cell Stem Cell* **2017**, *21*, 51–64. [[CrossRef](#)]
72. Wang, W.; Jin, S.; Ye, K. Development of Islet Organoids from H9 Human Embryonic Stem Cells in Biomimetic 3D Scaffolds. *Stem Cells Dev.* **2017**, *26*, 394–404. [[CrossRef](#)] [[PubMed](#)]
73. Kurmann, A.A.; Serra, M.; Hawkins, F.; Rankin, S.A.; Mori, M.; Astapova, I.; Ullas, S.; Lin, S.; Bilodeau, M.; Rossant, J.; et al. Regeneration of Thyroid Function by Transplantation of Differentiated Pluripotent Stem Cells. *Cell Stem Cell* **2015**, *17*, 527–542. [[CrossRef](#)] [[PubMed](#)]
74. Das, S.S.; Mishra, S.; Kaul, J.M. Development of Parafollicular Cells and their Relationship with Developing Thyroid Follicles in Human Foetuses. *J. Clin. Diagn. Res.* **2017**, *11*, AC01–AC04. [[CrossRef](#)] [[PubMed](#)]
75. Centeno, E.G.Z.; Cimarosti, H.; Bithell, A. 2D versus 3D human induced pluripotent stem cell-derived cultures for neurodegenerative disease modelling. *Mol. Neurodegener.* **2018**, *13*, 27. [[CrossRef](#)]
76. Reilly, G.C.; Engler, A.J. Intrinsic extracellular matrix properties regulate stem cell differentiation. *J. Biomech.* **2010**, *43*, 55–62. [[CrossRef](#)] [[PubMed](#)]